JOURNAL OF SPACECRAFT AND ROCKETS
Vol. 31, No. 4, July–August 1994

Arc Mitigation on High Voltage Solar Arrays

Renee Mong* and Daniel E. Hastings†
Massachusetts Institute of Technology, Cambridge, Massachusetts 02139

In response to the increasing demand for higher power sources in space, solar arrays are being designed with high voltages at low currents to meet this need. Unfortunately, negatively biased high voltage solar cells have been observed to arc when exposed to the low-Earth-orbit plasma environment. Analytical and numerical models of this arcing phenomenon for conventionally designed solar cells have been developed which show excellent agreement with experimental data. With an understanding of a mechanism for arcing, it is possible to assess mitigation strategies and quantify their effectiveness. It was determined that the arcing rate can be decreased by 1) increasing the interconnector work function, 2) increasing the thickness of the coverglass and cover adhesive, 3) decreasing the secondary electron yield of the coverglass and adhesive, 4) decreasing the ratio of the coverglass/adhesive dielectric constants, and 5) overhanging the coverglass. Of these, methods 4 and 5 show the most promise in mitigating or even eliminating arcing.

Nomenclature

A = $1.54 \times 10^{-6} \times 10^{4.52\,\phi_w^{1/2}}/\phi_w$, A/V^2
A_{cell} = solar cell frontal area m^2
B = $6.53 \times 10^9 \phi_W^{1.5}$, V/m
C_{diele} = capacitance of dielectric, F/m^2
d = thickness of dielectric, m
d_{gap} = gap distance between two cells, m
d_i = distance of electron first impact point from triple junction, m
d_o = overhang length of coverglass, m
d_o^c = critical overhang length of coverglass, m
d_1 = thickness of coverglass, m
d_2 = thickness of adhesive, m
E_i = electron incident energy on dielectric surface, eV
E_{max} = electron incident energy for maximum secondary electron yield, eV
E_{TJ} = electric field at triple junction, V/m
E_1 = electric field of coverglass, V/m
E_2 = electric field of adhesive, V/m
h = height of emission site from triple junction, m
j_{ec} = electron current density from the conductor, A/m^2
n_e = plasma density, m^{-3}
R = arc rate, s^{-1}
S_{FN} = emission site area at metal-dielectric interface, m^2
S_{real} = emission site area at dielectric-vacuum interface, m^2
V_{bias} = bias voltage of interconnector, V
V_i = intial voltage across dielectrics, V
v_{ion} = mean speed of ions entering sheath, m/s
β = field enhancement factor
γ_{ee} = secondary electron yield
γ_{max} = maximum secondary electron yield at normal incidence
ΔQ = charge lost from one coverglass by one discharge, C
ϵ_{d_1} = relative dielectric constant of coverglass
ϵ_{d_2} = relative dielectric constant of adhesive
η = ratio of electric field at emission site to electric field at triple junction
θ_i = incident impact angle of electron onto the dielectric surface, deg
ξ = factor accounting for difference of dielectric constants between coverglass and adhesive
τ_{arc} = time between arcs, s
τ_{efee} = enhanced field electron emission charging time, s
τ_{exp} = experiment time, s
τ_{ion} = ion charging time, s
ϕ_w = work function, eV

Received March 18, 1993; revision received Aug. 6, 1993; accepted for publication Aug. 11, 1993.

*Research Assistant, Department of Aeronautics and Astronautics.
†Professor of Aeronautics and Astronautics, Department of Aeronautics and Astronautics. Associate Fellow AIAA.

I. Introduction

CONVENTIONALLY, most solar array systems for space vehicles have a 28-V bus voltage. However, future solar arrays are being designed for much higher voltages to meet high power demands at low currents. High voltages are more desirable than high currents for attaining high power levels since this choice minimizes the resistive loss and the mass of the cables in the power distribution system. However, high voltage solar arrays have been observed to interact with the plasma environment of low Earth orbit in two distinct manners.[1-3] For positive voltage biases the current collection can be anomalously large, possibly leading to surface damage. For negative biases below a voltage threshold,[4] approximately −200 V, arc discharges can occur. Experimentally, an arc discharge on a solar cell has been defined as a sudden current pulse up to the order of one ampere and lasting a few microseconds or less. Arcing can cause electromagnetic interference with instruments and damage to the solar cells.[5] Thus, there is a design tradeoff between high voltages and damage from arcing unless solar cells can be designed to mitigate or even eliminate this arcing phenomenon.

Two different theories have been published to explain arcing on high voltage solar arrays. Jongeward et al.[6] proposed that there is a thin layer of insulating contaminant over the exposed interconnectors. Ions are attracted by the negative potential of the interconnectors and accumulate on the surface, resulting in the buildup of the electric field in the contaminant layer. The field causes electron emission into space, leading to subsequent heating and ionization in the layer. This positive feedback mechanism eventually culminates in an arc discharge. Hastings et al.[7] proposed that neutral gas molecules are caused to be desorbed from the sides of the coverglass by the prebreakdown current, which has been observed experimentally. The neutral molecules build up over the interconnectors. Inside this surface gas layer, arcing occurs as a flashover discharge.

Recent work by Cho and Hastings[8] combined some of the ideas from these two theories and studied the charging of the region near the plasma, dielectric, and conductor triple junction. The model that they studied is shown in Fig. 1. The dielectric consists of both the coverglass and the adhesive bonding of the coverglass to the solar cell. The conductor is the interconnector, which is usually placed between the cell and substrate on one

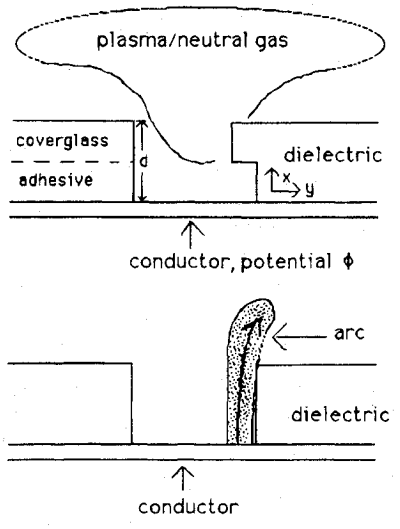

Fig. 1 Model system of the high-voltage solar array and plasma interaction.

end and between the cell and cover adhesive in the adjoining cell on the other end. The solar cell itself is neglected since the potential drop across it is at most a few volts whereas the potential drop across the coverglass and adhesive is hundreds of volts for high-voltage operation. This model system was designed to study conventional solar cells where the interconnector is exposed to space between the solar cells. It does not apply to the newer wrap through contact cells where the interconnector goes from the center of one cell to the next and is embedded in Kapton.

Cho and Hastings determined from theoretical and numerical work the following: 1) Ambient ions charge the dielectric front surface but leave the side surface effectively uncharged. 2) Ambient ions cause electron emission from the conductor. These electrons charge the side surface through secondary electron emission from the side surface to a steady state unless enhanced field electron emission (EFEE) becomes significant. 3) EFEE will charge the side surface if there is an electron emission site close to the triple junction with a high field enhancement factor β. 4) EFEE can result in collisional ionization of neutrals desorbed from the coverglass; this is the arc discharge. 5) The arc rate is the inverse of the sum of the ion and EFEE charging times. 6) For high voltages and high β values, the arc rate is mainly determined by the ion charging time; and for low voltages and low β values, the arc rate is dominated by the EFEE charging time.

Hastings et al.[9] extended this work to further develop the theory based on experimental work. Assuming a constant secondary electron yield and constant voltage level, they derived the following analytical expression for the EFEE charging time τ_{efee}:

$$\tau_{efee} = \frac{C_{diele} d_i^2}{(\gamma_{ee} - 1)\sqrt{S_{real}}\eta\xi A (S_{FN}/S_{real}) B\beta} \exp\left(\frac{Bd}{\beta V \eta \xi_0}\right) \quad (1)$$

where

$$\xi = \left[\frac{d_2}{d_i} + \frac{\epsilon_{d_2}}{\epsilon_{d_1}}\frac{d_1}{d_i}\right]^{-1} \quad (2)$$

and ξ_0 is ξ evaluated with $d_i = d$. For the ion charging process, each coverglass front surface is assumed to lose charge ΔQ in one arc discharge. This lost charge is replenished by ambient ions in time τ_{ion}. Then, τ_{ion} is given by

$$\tau_{ion} = \frac{\Delta Q}{e n_e v_{ion} A_{cell}} \quad (3)$$

The interval between arcs τ_{arc} is calculated by finding the minimum of the sum of τ_{ion} and τ_{efee}. This accounts for the fact that EFEE charging can be initiated whenever the conductor surface has a strong enough electric field, not just when the front surface current returns to near zero.

II. Numerical and Analytical Models

To determine how to mitigate arcing, the numerical and analytical models from Refs. 8 and 9 are used. The numerical model includes a particle in cell (PIC) code and a space-charge-free particle tracking code; the latter being used solely to save computational time. The PIC code is used for the ion charging of the front surface, and the particle tracking code is used for the charging of the dielectric by electrons from the conductor. The computational domain is two-dimensional with three-dimensional velocities. The boundary conditions are periodic in the y direction and Dirichlet in the x direction. The particle tracking code progresses until the electric field runs away or assumes a steady state. A run-away electric field is taken to imply that an arc discharge has been initiated. Although the electron current associated with a run-away electric field may cause a breakdown in the desorbed neutral gas or dielectric, it is possible that the current will become space-charge limited before a breakdown can occur.[10] Therefore, counting an arc whenever the field starts to run away will provide an upper bound on the arc rate.

The analytical model, which is used to calculate the arc rates, is based on the theory of Cho and Hastings.[8] The arcing rate is calculated by dividing the number of arcs during a finite experiment time by the experiment time. The time between arcs τ_{arc} is the shortest charging time, $\tau_{efee} + \tau_{ion}$, among all of the emission sites on the interconnector surface. The minimum time for each site is determined by solving for the voltage which gives the minimum τ_{arc}. The voltage varies from V_i, the voltage between the coverglass front surface and the conductor just after the arc, and V_{bias}. If the voltage is neither V_i or V_{bias}, the solution is determined by the Newton-Raphson method. After τ_{arc} has been determined, it is compared with the experiment time τ_{exp}. If τ_{exp} is greater, another τ_{arc} is calculated until the sum of arcing times is greater than τ_{exp}. For experiments and real systems, some parameters that determine the arc charging time will likely not be known exactly but rather as a distribution with some statistical variation. To choose these parameters for the model, each is chosen from a probability distribution function given a defined range of values. These parameters are the emission site height h, the first impact point d_i, the electric field correction factor η, the real emission site area S_{real}, the emission site area determined from Fowler-Nordheim plot S_{FN}, the charge lost in a discharge ΔQ, n_e, and the enhancement factor β.

Hastings et al. use this procedure in Ref. 9 to calculate the arc rate numerically for the PIX II flight and ground experiments as well as the SFU ground experiments. The results show good agreement with the data over the range for which the data exists. This agreement and the understanding of the processes governing the arcing allows us to assess mitigation strategies and design modifications to conventional solar cells.

III. Increasing the Electric Field Charging Time

In this paper we consider several methods of reducing the arc rate. Since τ_{ion} is dependent mainly on mission parameters such as n_e and v_{ion}, all of the methods we shall try concern increasing τ_{efee}, which is affected only by cell properties. Some property variations are shown to have results which can be predicted well by using the analytic expression given by Eq. (1). Other property variations are shown to have results which are represented in the analytic expression but are not as easily predicted. In addition, we consider lengthening the coverglass

over the interconnector to obstruct the electron trajectories, a method which can not be predicted at all by the analytic expression.

The cell used as the control case for these arc rate simulations is the silicon conventional cell without a coverglass overhang. The input parameters chosen to simulate this cell are shown in Table 1. The dielectrics are a fused silica coverglass and DC 93500 adhesive, and the interconnector material is the alloy Kovar. The interconnector work function is taken to be the weighted average of the work functions of the elements which compose it. For all numerical simulations the domain size used is 3 mm in the x direction and 2.5 mm in the y direction, which includes one-half of two 2-mm-wide cells and a 0.5-mm gap in between them. All simulations assumed the same environment of $n_e = 5 \times 10^{11}$ m^{-3}, electron and ion temperatures of 0.1 eV, kinetic energy of incoming ions of 5 eV, and a 90-deg orientation to the ram velocity. In addition, the emission site on the conductor was set adjacent to the triple junction with an area of 1.2×10^{-13} m^2. This corresponds to a submicron size dielectric emission site up against the triple junction. Since EFEE charging is dependent on an emission site near the triple junction, this condition will define the lower bound for τ_{efee} and the upper bound for the arc rate.

A. Interconnector Material

The work function of the electron emitting surface determines the ease with which electrons are released. If the number of electrons emitted from the interconnector is reduced, the time for the electric field at the triple junction to build up will be increased. In the analytical formula for τ_{efee}, the work function determines the value of the Fowler-Nordheim coefficients A and B. Figure 2 shows τ_{efee} plotted against βV over a range of significant values. The charging time τ_{efee} is plotted against βV in Fig. 2 since the analytic theory[9] indicates that τ_{efee} is exponentially dependent on βV. As expected, metals with work functions higher than the control case of 4.76 eV have longer times for EFEE charging, and metals with lower work functions have shorter times. The numerical simulation results can be easily predicted from the analytic theory. To determine the effect of a different work function ϕ_{w2}, we can solve the ratio $\tau_{efee}(\phi_{w2})/\tau_{efee}(\phi_w)$ using Eq. (1). The only unknown variable is η, which is within the range 1.001–1.005 for emission sites adjacent to the triple junction. For the cases shown in Fig. 2, this expression is evaluated and plotted with the equivalent numerical values in Fig. 3. The predictions are all within the margin of error for the analytical and numerical values, except for the extreme case of $\phi_w = 5.9$ eV for which the analytical result is too high. For this case where the initial currents are very low, the assumption in the analytic model of a secondary electron emission independent of energy makes the model underestimate the effects of the secondary electrons.

Table 1 Conventional silicon cell data used in numerical simulation

d_1, mm	d_2, mm	ϵ_{d_1}	ϵ_{d_2}	γ_{max1}	γ_{max2}	E_{max1}, V	E_{max2}, V	d_{gap}, mm	ϕ_w, eV
0.153	0.037	3.5	2.7	3.46	3.0	330	300	0.5	4.76

B. Dielectric Thickness

Another method of potentially modifying the arc rate is to increase the dielectric thickness, $d = d_1 + d_2$. This lowers the voltage drop for a given height from the interconnector and reduces the energy with which primary electrons strike the side surface. The analytic theory[9] accounts for changes in thickness in the exponential factor of τ_{efee}. The exponential factor also includes ξ, which is dependent on the ratio of dielectric thicknesses, d_1/d_2. To exclude this factor, the ratio is the same for each case studied. Further simulations which studied the effect of this ratio showed that it did not alter the results. Figure 4

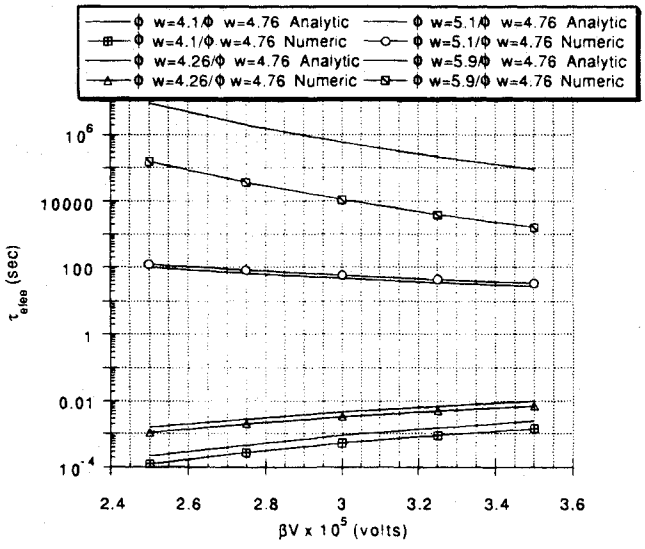

Fig. 3 Analytic predictions and numerical results for $\tau_{efee}/\tau_{efee}(\phi_w = 4.76$ eV) vs βV.

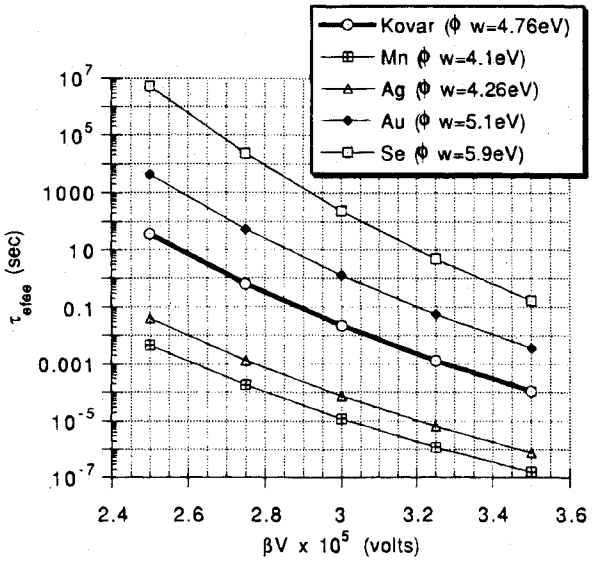

Fig. 2 Enhanced field electron emission charging time τ_{efee} vs βV for different work functions ϕ_w eV.

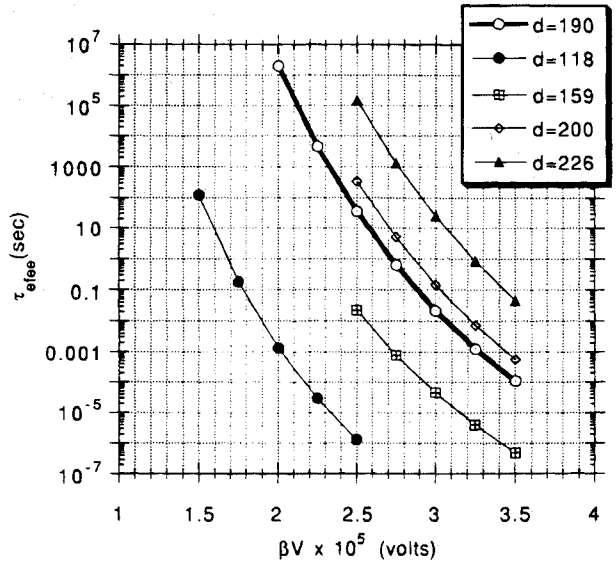

Fig. 4 Enhanced field electron emission charging time τ_{efee} vs βV for different dielectric thicknesses d μm.

shows τ_{efee} plotted against βV for the control case and for four cases with differing thicknesses. As expected, increases in thickness increase τ_{efee} significantly. The change in τ_{efee} can again be easily predicted by calculating the ratio of $\tau_{efee}(d + \Delta d)/\tau_{efee}(d)$ using Eq. (1). The analytic results are plotted with the numerical results in Fig. 5. The predictions are all within the accuracy of the numerical simulations. The prediction for the largest variation of $d = 118$ μm is only off by a factor of three. Using the same control case, an increase in thickness to 250 μm would result in an increase in τ_{efee} of nearly six orders of magnitude. This will effectively eliminate electric field run away. However, a decrease in thickness to 50 μm would result in a decrease in τ_{efee} of nearly 14 orders of magnitude. In this case the arc rate will be dominated by the ion recharging time.

C. Secondary Electron Yield

The secondary electron yield γ_{ee} from the dielectrics must on the average be greater than unity for the electric field to build up and run away. If γ_{ee} is equal to unity, the electric field will assume a steady state and no charge accumulation will occur. If γ_{ee} is less than unity, the electric field will decrease as a negative charge accumulates on the dielectrics. This is modeled in Eq. (1) by the factor $(\gamma_{ee} - 1)^{-1}$. A numerical sensitivity scan of τ_{efee} over relevant values of βV for γ_{ee} values of actual materials is shown in Fig. 6. As in the previous scans, only the property of interest γ_{ee} is varied from the control case. In these cases, γ_{ee} is the same for both dielectrics, although the control case has slightly different values of γ_{ee} for the two dielectric materials, fused silica and DC 93500. To choose relevant values, the following expression for γ_{ee} (Ref. 11) is evaluated for different γ_{max} and E_{max} values determined for actual materials:

$$\gamma_{ee} = \gamma_{max}\frac{E_i}{E_{max}}\exp\left(2 - 2\sqrt{\frac{E_i}{E_{max}}}\right)\exp[2(1 - \cos\theta_i)] \quad (4)$$

This expression is good up to impact energies E_i of about 1 keV where

$$E_i = \frac{\xi_0}{\xi}V\frac{d_i}{d} \quad (5)$$

and $\theta_i = \arctan(d_i/y)$, with y being the distance of the emission site from the triple junction. The range of values shown for the yield of the materials is determined from the numerical results

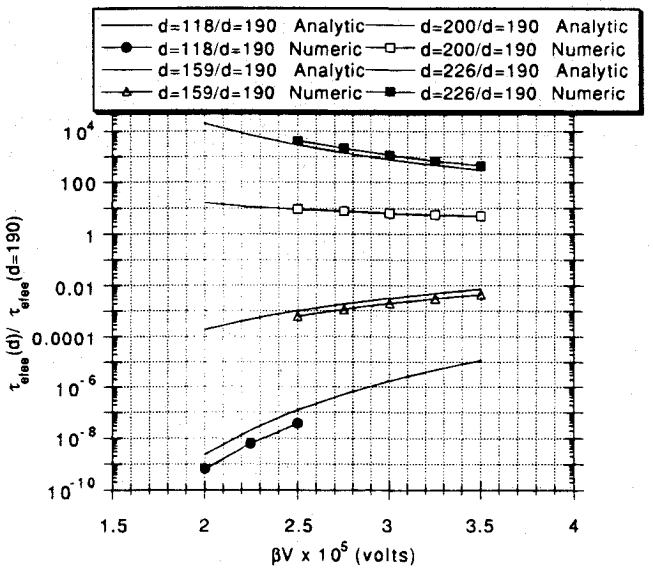

Fig. 5 Analytic predictions and numerical results for τ_{efee}/τ_{efee} (d = 190 μm) vs βV.

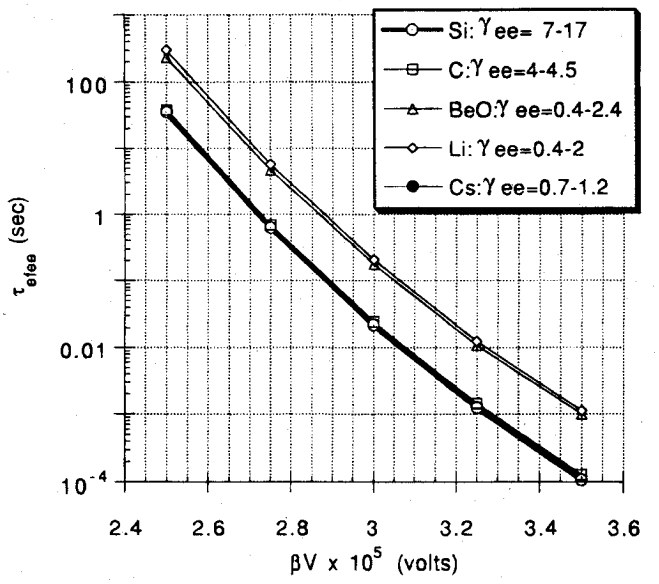

Fig. 6 Enhanced field electron emission charging time τ_{efee} vs βV for different secondary electron yields γ_{ee}.

when the appropriate values for γ_{max} and E_{max} are used. As expected, materials with secondary electron yields nearer unity have much longer times for the electric field to run away. Indeed, for cesium the electric field never runs away in the simulations. In the analytic formula, which assumes an energy and angle independent yield, the run-away time scales as $(\gamma_{max} - 1)^{-1}$. This simple scaling is unable to predict the results in Fig. 6.

D. Dielectric Constants

Although the effect of different dielectric constants is not as apparent in the analytical formula as are the other cell properties, it does significantly affect the surface charge density and consequently, the secondary electron yield. Since $\epsilon_{d_1} E_1 = \epsilon_{d_2} E_2$, the ratio of dielectric constants, $\epsilon_{d_1}/\epsilon_{d_2}$, must equal the ratio of electric fields, E_2/E_1. Therefore, if $\epsilon_{d_1}/\epsilon_{d_2}$ is greater than one, the electric field on the lower side surface will be higher. The higher electric field results in a higher surface charge density causing more electrons to be attracted and many more secondary electrons to be emitted. The electric field at the triple junction should build up quite rapidly causing τ_{efee} to be relatively short. If $\epsilon_{d_1}/\epsilon_{d_2}$ is less than one, the electric field on the lower surface will be lower than the electric field on the upper surface, so that it is very difficult for the electric field to build up at the triple junction. The time τ_{efee} should then be very long. Analytically, the ratio of $\epsilon_{d_1}/\epsilon_{d_2}$ in Eq. (2) determines whether ξ_0 is less than, equal to, or greater than 1. This has a considerable affect on γ_{ee} through E_i as shown in Eq. (4). The effect on the surface charge density is not accounted for, however, as the analytic expressions do not predict the large variation of τ_{efee} calculated by the numerical simulations. The numerical results are shown in Fig. 7. By increasing the ratio $\epsilon_{d_1}/\epsilon_{d_2}$ from the control case of 1.3 to 2.7, τ_{efee} decreases by about seven orders of magnitude. By decreasing the ratio from 1.3 to 0.74, τ_{efee} increases by about 12 orders of magnitude. As expected, these results can be explained by the surface charge density. The numerical results of the surface charge density calculations are shown in Fig. 8. For higher values of $\epsilon_{d_1}/\epsilon_{d_2}$, the surface charge density is correspondingly high over the lower dielectric side surface, causing the electric field to run away in a short time. For the control case, the surface charge density does not build up as high before the EFEE charging so τ_{efee} is longer. For cases with $\epsilon_{d_1}/\epsilon_{d_2} < 1$, the surface charge density over the lower dielectric side surface is negative before beginning EFEE charging so that electrons are repelled from the adhesive, causing secondary electron emission to be severely reduced. For these

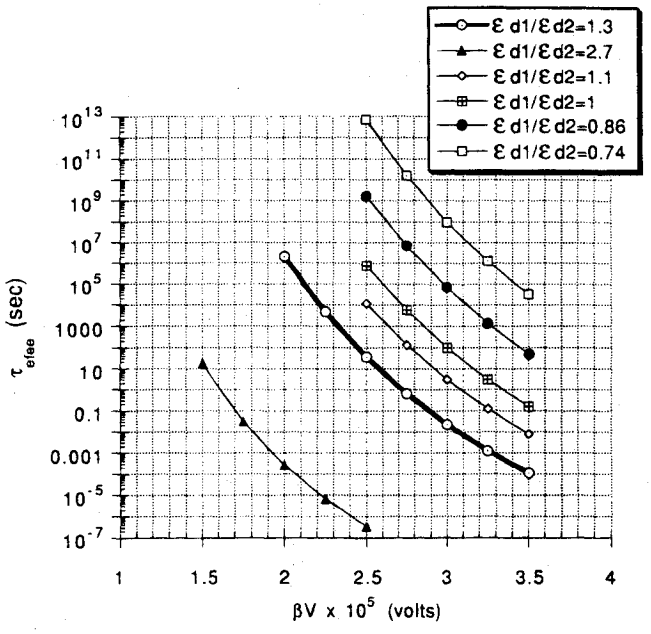

Fig. 7 Enhanced field electron emission charging time τ_{efee} vs βV for different dielectric constant ratios.

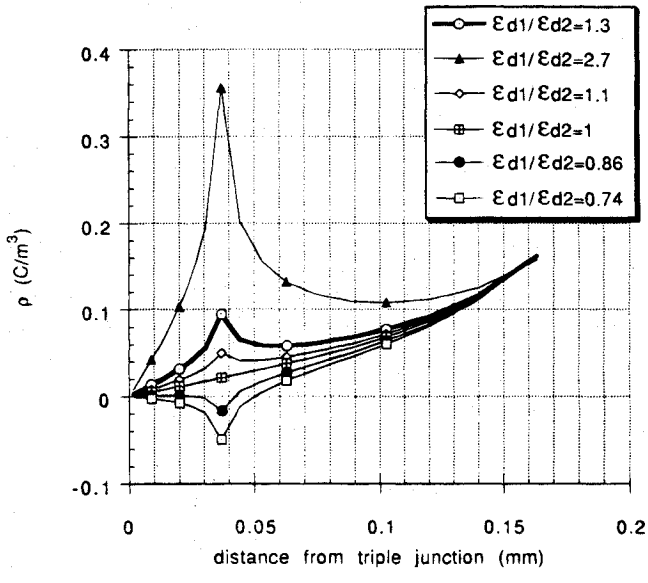

Fig. 8 Dielectric side surface charge density before EFEE charging for different dielectric constants.

cases the useful secondary electron yield is near or below 1, so that the electric field assumes a steady state, which does not run away in any reasonable time.

E. Overhanging the Coverglass

The final mitigation strategy included involves lengthening the coverglass into an overhang over the interconnector to create a back surface on which charge can accumulate. This method is expected to increase τ_{efee} since the overhang creates an additional surface over which the charge must build up for the electric field to run away. This was examined in Ref. 12 and the results confirm this expectation. As the overhang is increased in length up to 30 μm, τ_{efee} is increased uniformly. In the βV range studied (see Fig. 9), this pattern changes for overhangs longer than 30 μm, indicating a different physical effect of the overhang on the EFEE charging time.

The results suggested that there is a critical overhang which determines the behavior of the solution. Below this critical overhang, the electric field run away is similar to the case of

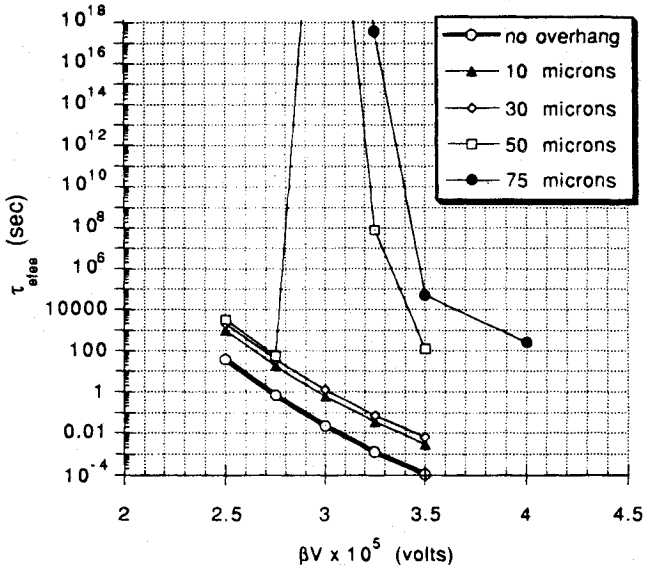

Fig. 9 Enhanced field electron emission charging time τ_{efee} vs βV for different overhangs d_o.

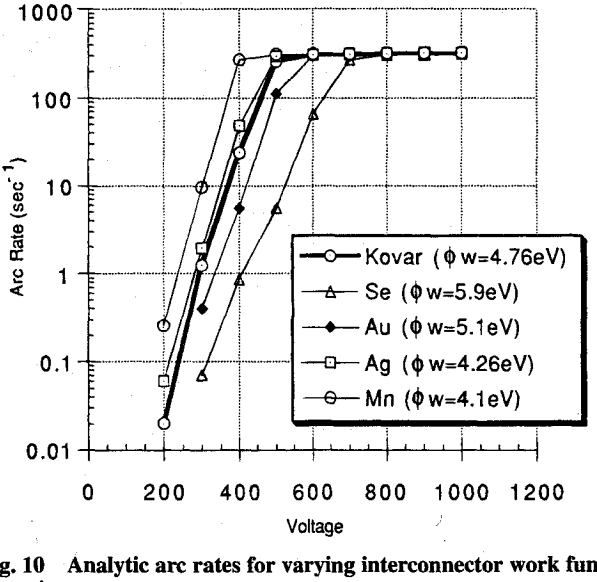

Fig. 10 Analytic arc rates for varying interconnector work functions ϕ_w.

no overhang but at a delayed time. Above it, the field initially decreases for a long time before building up to the run away. Hence, coverglasses made longer than this critical overhang will have substantially reduced arcing.

Using the geometry shown in Fig. 1, it was shown in Ref. 12 that the critical overhang d_o^c could be written approximately as

$$d_0^c \leq \frac{4\mathscr{E}_1 \epsilon_{d_2}}{eV_{\text{bias}}\epsilon_{d_1}} d_1 \tag{6}$$

where $\mathscr{E}_1$ is the energy at which the secondary electron yield is unity. This shows that one can obtain the smallest critical overhang by reducing d_1 as much as possible, consistent, of course, with the need to maintain radiation protection and by modifying the secondary electron emission properties of the coverglass so as to reduce the energy at which the yield is unity.

IV. Arc Rate Results

The analytical model discussed in Sec. II was used to determine the arc rates for each variation considered in the previous

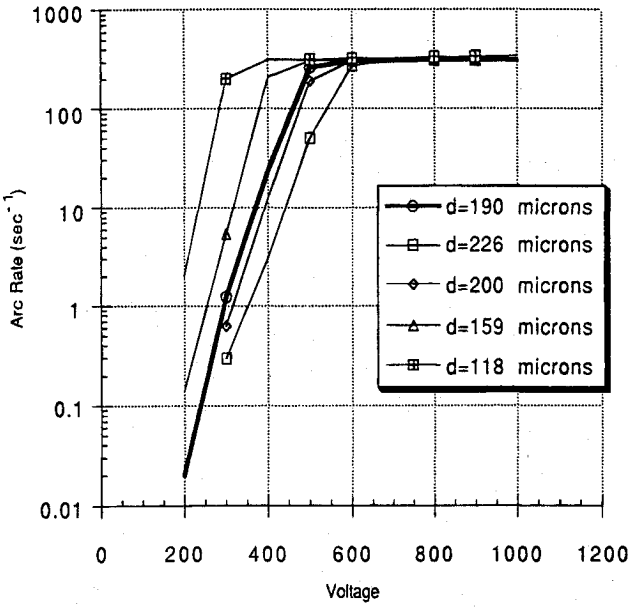

Fig. 11 Analytic arc rates for varying dielectric thicknesses *d*.

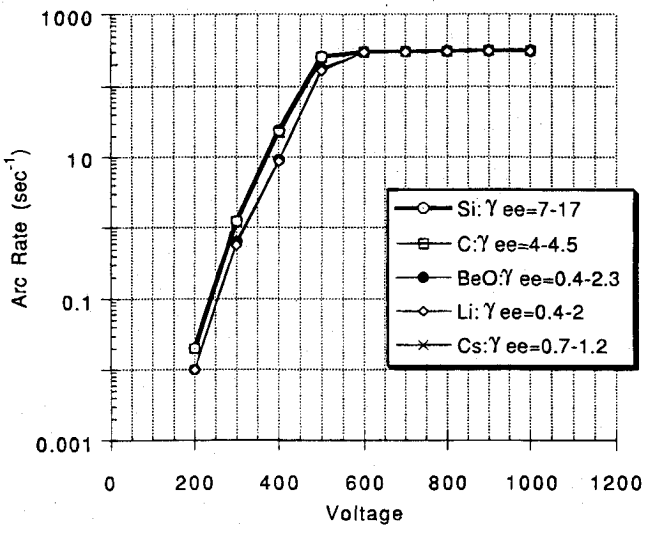

Fig. 12 Predicted arc rates for varying secondary electron yields τ_{ee}.

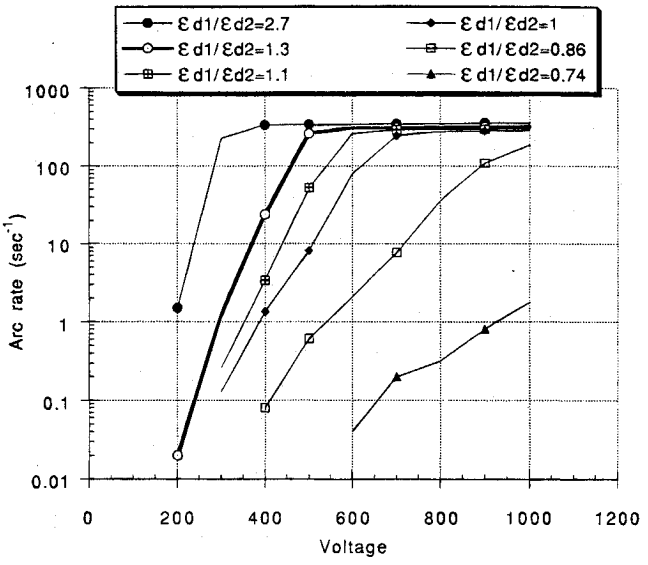

Fig. 13 Predicted arc rates for varying dielectric constant ratios $\epsilon_{d_1}/\epsilon_{d_2}$.

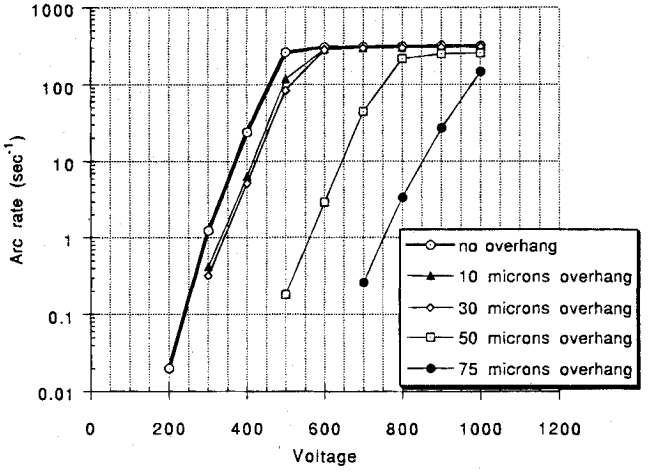

Fig. 14 Predicted arc rates for varying coverglass overhang lengths d_o, μm.

section. In this model, the arcing time is determined by the one emission site on a conductor of typically 1000 sites which has the shortest charging time of all of the cells. This is a more realistic simulation than the numerical simulations in which only the effect of one site on one conductor was studied. However, this model is limited by the analytic expressions, which are only approximations of real processes and effects. For the changes which are consistent with the analytic predictions, the model is used with the varying parameters. For the secondary electron yield, dielectric constant, and overhang effects on τ_{efee}, which are not fully accounted for in the analytic expression, the model is used with τ_{efee} modified according to the results from the numerical simulations.

The results are shown in Figs. 10–14. In all cases the curves saturate around 350 s^{-1}, where the arc rate is limited by τ_{ion} which is not as dependent on voltage as is τ_{efee}. The arc rate plot with different work functions shows that only in the extreme cases does the arc rate change significantly. The thickness variations show a greater effect on the arc rate, especially for the smaller thicknesses from −200 to −400 V. The effect of the secondary electron yield on the arc rate is shown only to be significant when the electric field does not run away, as in the γ_{ee} = 0.7–1.2 case. The dielectric constant variations and coverglass overhang cases show the largest effect on the arc rate. For the $\epsilon_{d_1}/\epsilon_{d_2}$ = 2.7 case, the arc rate is almost saturated at −300 V. For the case of equal dielectric constants, however, the arc rate does not saturate until −900 V. For variations of $\epsilon_{d_1}/\epsilon_{d_2} < 1$ the arc rate is reduced severely. No arcing is predicted until −600 V for the $\epsilon_{d_1}/\epsilon_{d_2}$ = 0.74 case. For the coverglass overhang arc rates, the two different classes can be clearly seen. The arc rates of the first class do not decrease much even with an overhang of 30 μm, but the arc rates of the second class are significantly reduced. The 75-μm case, which is beyond the critical overhang for the cell studied, shows no arcing until −600 V and does not reach the saturation level in the range of voltages examined.

V. Conclusions

By using numerical and analytical models of arcing on high-voltage solar arrays the following methods were found to decrease the arc rate: 1) increase the interconnector work function; 2) increase the dielectric thickness; 3) decrease the secondary electron yield to near or below 1; 4) decrease the ratio $\epsilon_{d_1}/\epsilon_{d_2}$, especially to below 1; and 5) overhang the coverglass, particularly past the critical overhang which causes electrons to be trapped on the coverglass back surface. Increasing the work function affects τ_{efee} significantly, but only affects the arc

rate for extreme values. The dielectric thickness has a slightly larger effect on the arc rate, particularly for low thicknesses and low voltages. The secondary electron parameters which eliminate the electric field run away eliminate arcing. The best results for decreasing the arc rate are achieved by changing the dielectric constants and by extending the coverglass over the interconnector.

Acknowledgment

This work was supported by the Air Force under Grant AFOSR-87-0340.

References

[1] Herron, B. G., Bayless, J. R., and Worden, J. D., "High Voltage Solar Array Technology," *Journal of Spacecraft and Rockets*, Vol. 10, 1973, p. 457.

[2] Stevens, N. J., "Review of Interactions of Large Space Structures with the Environment," *Space Systems and their Interactions with Earth's Space Environment*, Progress in Aeronautics and Astronautics, Vol. 71, AIAA, Washington, DC, 1980. pp. 437–454.

[3] Thiemann, H., and Bogus, K., "Anomalous Current Collection and Arcing of Solar-Cell Modules in a Simulated High-Density Low-Earth-Orbit Plasma," *European Space Agency Journal*, Vol. 10, 1986, pp. 43–57.

[4] Grier, N. T., "Plasma Interaction Experiment II: Laboratory and Flight Results," *Spacecraft Environment Interactions Technology Conference* (Colorado Springs, CO), NASA CP-2359, 1983 pp. 333–348.

[5] Thieman, H., Schunk, R. W., and Bogus, K., "Where Do Negatively Biased Solar Arrays Arc?," *Journal of Spacecraft and Rockets*, Vol. 27, 1990, pp. 563–565.

[6] Jongeward, G., Katz, I., Mandell, M., and Parks, D. E., "The Role of Unneutralized Surface Ions in Negative Potential Arcing," *IEEE Transactions on Nuclear Science*, Vol. NS-32, No. 6, 1985.

[7] Hastings, D. E., Weyl, G., and Kaufman, D., "The Threshold Voltage for Arcing on Negatively Biased Solar Arrays," *Journal of Spacecraft and Rockets*, Vol. 27, 1990, pp. 539–544.

[8] Cho, M., and Hastings, D. E., "Dielectric Charging Processes and Arcing Rates of High Voltage Solar Arrays," *Journal of Spacecraft and Rockets*, Vol. 28, No. 6, 1991, pp. 698–706.

[9] Hastings, D. E., Cho, M., and Kuninaka, H., "The Arcing Rate for a High Voltage Solar Array: Theory, Experiments, and Predictions," *Journal of Spacecraft and Rockets*, Vol. 29, No. 4, 1992, pp. 538–554.

[10] Cho, M., and Hastings, D. E., "Dielectric Charging Processes and Arcing Rates of High Voltage Solar Arrays," *Journal of Spacecraft and Rockets*, Vol. 30, No. 2, 1993, pp. 189–201.

[11] Hachenberg, O., and Brauer, W., "Secondary Electron Emission from Solids," *Advances in Electronics and Electron Physics*, Vol. 11, 1959, pp. 413–499.

[12] Hastings, D. E., Cho, M., and Mong, R., "Implications for the Technology of High Voltage Solar Arrays: The Possibility of an Arc Resistant Cell," *Acta Astronautica*, Vol. 30, No. 1, 1993, pp. 115–125.

Alfred L. Vampola
Associate Editor